Detailed Structural Characterization of Unbound Protein Phosphatase 1 Inhibitors[†]

Barbara Dancheck,[‡] Angus C. Nairn,[§] and Wolfgang Peti*[,‡]

Department of Molecular Pharmacology, Physiology and Biotechnology, Brown University, Providence, Rhode Island 02912, and Department of Psychiatry, Yale University School of Medicine, New Haven, Connecticut 06508

Received July 11, 2008; Revised Manuscript Received September 29, 2008

ABSTRACT: Protein phosphatase 1 (PP1) is an essential and ubiquitous serine/threonine protein phosphatase that is regulated by more than 100 known inhibitor and targeting proteins. It is currently unclear how protein inhibitors distinctly and specifically regulate PP1 to enable rapid responses to cellular alterations. We demonstrate that two PP1 inhibitors, I-2 and DARPP-32, belong to the class of intrinsically unstructured proteins (IUPs). We show that both inhibitors have distinct preferences for transient local and long-range structure. These preferences are likely their structural signature for their interaction with PP1. Furthermore, we show that upon phosphorylation of Thr^{34} in DARPP-32, which turns DARPP-32 into a potent inhibitor of PP1, neither local nor long-range structure of DARPP-32 is altered. Therefore, our data suggest a role for these transient three-dimensional topologies in binding mechanisms that enable extensive contacts with PP1's invariant surfaces. Together, these interactions enable potent and selective inhibition of PP1.

The two distinct types of enzymes that are capable of transient covalent modifications of proteins are kinases and phosphatases. However, while the human genome encodes an almost equal number of tyrosine (tyr) kinases and phosphatases (90 vs 107), there is a dramatic disparity between the number of serine/threonine (ser/thr) kinases and phosphatases (428 vs ~40) (*1*). This suggests that ser/thr phosphatases might be more promiscuous than tyr phosphatases, yet are presumably under strict temporal and spatial control. Protein phosphatase 1 (PP1)[1] (*2*) is an essential ser/thr phosphatase found in all tissues with roles in cellular processes as diverse as cell cycle progression, protein synthesis, muscle contraction, carbohydrate metabolism, transcription, and neuronal signaling. Because of its diverse roles, PP1 must be active toward a broad range of substrates while maintaining specificity. Its activity is under exceedingly tight and specific control; it is regulated by more than 100 inhibitor and targeting proteins, with predictions of up to 200 (*3*−*5*).

Two types of PP1 inhibitors are currently known: protein-based inhibitors and natural small molecular toxin inhibitors, such as microcystin-LR or tautomycin (*6, 7*). Most small molecular toxin inhibitors are potent against PP1, PP2A, and to some degree PP2B (the two related members of the PPP family of ser/thr protein phosphatases). This is not the case for protein-based inhibitors, which are specific for a single PPP family member and are the focus of our work. Inhibitor proteins themselves come in two categories: pseudosubstrate inhibitors, which require phosphorylation to become potent inhibitors, and inhibitors that are potent without phosphorylation. Both types of inhibitors specifically bind PP1 and block its activity. A PP1 interaction motif [$(R/K)x_1x_2x_3(F/W)$] has been identified as a requirement for PP1 binding (*5*). However, the presence of this motif alone is not adequate to confer binding to PP1. Therefore, it has been suggested by numerous PP1 research groups that regions outside of this interaction site are essential for PP1 regulation and that these regions provide the necessary specificity in the PP1−regulator interaction. Crystal structures of PP1 in complex with molecular toxins such as microcystin-LR (*8*−*10*), a peptide from the glycogen regulating subunit (*11*), and the MYPT1 regulatory subunit (*12*) have been reported. These structures show that the active site of PP1, which is directly targeted by PP1 inhibitors, is more than 20 Å from the common PP1 interaction site. Despite differences in the PP1 isoforms crystallized, crystallization conditions used, and crystal packing contacts observed, PP1's overall structure is highly invariable. The only reported exception is an interaction of seven C-terminal PP1 residues with the ankyrin repeats in the PP1−MYPT1 regulatory subunit complex, which become structured upon interaction with PP1δ (*12*). Therefore, it has been established that inhibitor proteins contact distal sites in PP1 simultaneously.

Here, we studied the three-dimensional (3D) structures of two biologically important PP1 inhibitors. First, DARPP-32 (dopamine- and cyclic AMP-regulated phosphoprotein with

[†] This material is based upon work supported by a National Science Foundation Graduate Research Fellowship to B.D. The project described was supported by Grant R01NS056128 from the National Institute of Neurological Disorders and Stroke to W.P. and by Grant P50 MH074866 from the National Institute of Mental Health to A.C.N. Some NMR data were recorded on the Bruker AVANCE II 800 MHz spectrometer at Brandies University (NIH Grant S10-RR017269). The CD spectrometer is part of the RI-EPSCoR Proteomics Facility which is supported by the National Science Foundation under Grant 0554548 and by NIH NCRR Grant 1S10RR020923. The DLS is supported by a Seed-Fund grant from the Office of the Vice President of Research at Brown University. W.P. is the Manning Assistant Professor for Medical Science at Brown University.

* To whom correspondence should be addressed. Phone: (401) 863-6084. Fax: (401) 863-6087. E-mail: wolfgang_peti@brown.edu.

[‡] Brown University.

[§] Yale University School of Medicine.

[1] Abbreviations: PP1, protein phosphatase 1; NMR, nuclear magnetic resonance; IUP, intrinsically unstructured proteins; DARPP-32, dopamine- and cyclic AMP-regulated phosphoprotein with molecular weight 32 kDa; I-2, inhibitor-2.

10.1021/bi801308y CCC: $40.75
Published on Web 10/28/2008

molecular weight of 32 kDa) is a PP1 inhibitor enriched in the striatum that requires phosphorylation at Thr^{34} to become active as a pseudosubstrate inhibitor (*13, 14*). The phosphorylation state of DARPP-32 Thr^{34} is controlled by protein kinase A (PKA) and calcineurin, which are themselves individually upregulated by various neurotransmitter pathways in striatal neurons. Thus, DARPP-32 is a key component in the integration of multiple signaling pathways in the brain (*14*). Second, I-2 (inhibitor-2) is a PP1 inhibitor that does not require phosphorylation to achieve inhibition (*4, 15*−*18*). I-2 is ubiquitously expressed, though its level and cellular localization fluctuate during the cell cycle, suggesting a role in cell division. *In vitro*, I-2 forms an inactivate complex with PP1, which can be reactivated by phosphorylation of Thr^{72} on I-2 (GSK-3) without the release of I-2 (*19*). Although this reactivated complex has not yet been demonstrated in vivo, phosphothreonine I-2 has been found in vivo, and a GSK-3−PP1−I-2 complex has been found in cells overexpressing these three proteins (*16, 20*). The sequential backbone assignments of similar DARPP-32 (*21*) and I-2 (*22*) constructs, as well as the equally important PP1−I-2 crystal structure (*23*), were recently published.

In this study, we characterized the unbound states of I-2_{9-164} and DARPP-32_{1-118} at atomic resolution. Additionally, as DARPP-32 must be phosphorylated at Thr^{34} for PP1 inhibition, we characterized the unbound form of Thr^{34}-phosphorylated DARPP-32_{1-118} (pDARPP-32_{1-118}). We leverage our data by direct comparison with biochemical data reported in the literature for the interactions of these regulators with PP1. Thus, studying these PP1 inhibitors at atomic resolution enables a detailed comparison of their unstructured states and, more importantly, enables us to propose likely scenarios for their binding interactions with PP1. We show that their inherent characteristics, namely, high flexibility and discernible structural preferences in regions biochemically identified as being important for their interactions with PP1, are likely important determinants for the specificity of their different interactions with PP1. Lastly, our data also show that Thr^{34} phosphorylation of DARPP-32_{1-118} does not affect local transient structure and dynamics, or long-range contacts present in its unbound state.

MATERIALS AND METHODS

Inhibitor Expression and Purification. Constructs representing the biochemically identified PP1 binding domains of human I-2_{9-164} and rat DARPP-32_{1-118} C72S (*21, 22*) were subcloned into a pET28a-modified vector which encodes a $Thio_6His_6$ expression/purification tag and a TEV (tobacco etch virus protease) cleavage site (*24*). The C72S mutation of DARPP-32_{1-118} was created because wild-type DARPP-32_{1-118} readily formed a dimer in solution, as shown by analytical size exclusion chromatography (Superdex 200 10/300 GL, GE Healthcare) (data not shown). The plasmids were transformed into *Escherichia coli* strain BL21-CodonPlus (DE3)-RIL (Stratagene). The expression of uniformly ^{13}C- and/or ^{15}N-labeled protein was carried out by growing freshly transformed cells in M9 minimal medium containing 4 g/L [^{13}C]-D-glucose and/or 1 g/L $^{15}NH_4Cl$ (CIL) as the sole carbon and nitrogen sources, respectively, after induction with 1 mM IPTG.

All cells were lysed by high-pressure homogenization (Avestin C-3 Emulsiflex). For the first purification step, the soluble proteins were loaded onto a HisTrap HP column (GE Healthcare) and were eluted with an imidazole gradient. Fractions containing the proteins were pooled, dialyzed into fresh buffer, and incubated with TEV NIa (S219V) protease fused to an in-frame His_6 tag until cleavage was complete. The samples were then loaded onto a Ni-NTA column (Invitrogen) from which they eluted in the flow through. For the final purification step, the proteins were loaded onto either a Superdex 75 26/60 or 16/60 size exclusion column (GE Healthcare) equilibrated with 20 mM sodium phosphate buffer (pH 6.5) and 50 mM NaCl (I-2_{9-164}) or with 50 mM sodium phosphate buffer (pH 5.5) and 50 mM NaCl (DARPP-32_{1-118}). Fractions containing the pure proteins, as confirmed by SDS−PAGE, were pooled and concentrated to 0.75 mM. Phenylmethanesulfonyl fluoride (PMSF) (0.25 mM) was added as a protease inhibitor, and 10% D_2O was added for NMR experiments.

The activity of the purified proteins was tested by their ability to form complexes with recombinantly expressed PP1, as seen with size exclusion chromatography (Superdex 75 26/60, GE Healthcare; Supporting Information). Expression and purification of PKA are also described in the Supporting Information.

Phosphorylation of DARPP-32_{1-118}. Purified DARPP-32_{1-118} was exchanged into a pH 8.4 buffer for phosphorylation. The final reaction conditions included 20 mM Tris (pH 8.4), 50 mM NaCl, 200 μM ATP, 10 mM $MnCl_2$, 1 mM EDTA, and 8 μg/mL PKA. Stoichiometric phosphorylation of DARPP-32_{1-118} at Thr^{34} occurred in 90 min at 30 °C and was confirmed by mass spectrometry. Following phosphorylation, pDARPP-32_{1-118} was loaded onto a Superdex 75 26/60 size exclusion column (GE Healthcare) equilibrated with 50 mM sodium phosphate buffer (pH 5.5) and 50 mM NaCl. Fractions containing the pure protein, as confirmed by SDS−PAGE, were pooled and concentrated to 0.55 mM (^{13}C- and ^{15}N-labeled sample) or 0.75 mM (^{15}N-labeled sample). PMSF (0.25 mM) was added as a protease inhibitor, and 10% D_2O was added for NMR experiments.

Generation of Cysteine Mutants and Spin Labeling. The QuikChange site-directed mutagenesis kit (Stratagene) was used to create the C72S single mutant and the G5C/C72S, A36C/C72S, S51C/C72S, and S94C/C72S double mutants of DARPP-32_{1-118}, as well as the G12C/C85S, D47C/C85S, S121C/C85S, and N152C/C85S double mutants of I-2_{9-164}, following the manufacturer's protocol. The presence of the mutations was confirmed by sequencing analysis.

(1-Oxyl-2,2,5,5-tetramethyl-3-pyrroline-3-methyl)methanethiosulfonate (MTSL) (Toronto Research Chemicals) was covalently linked to single cys residues by incubating the proteins with MTSL overnight. $^1H-^{15}N$ HSQC spectra were recorded for the proteins in a buffer with DTT before MTSL incubation; the sample was then quickly exchanged into the same buffer without DTT using a HiPrep 26/10 desalting column (GE Healthcare) immediately before incubation with MTSL. To remove free MTSL, the proteins were purified by size exclusion chromatography (Superdex 75 26/60 or 16/60, equilibrated with their typical NMR buffers). Spin-label incorporation for most samples was confirmed by mass spectrometry (Voyager Pro DE MALDI-TOF mass spectrometer, Applied Biosystems) and dynamic light scattering

(see below); two-dimensional (2D) $^{1}H-^{15}N$ HSQC spectra of the samples before and after spin-label incorporation ensured that the label did not perturb the overall structure of the proteins (Supporting Information). Results were within experimental error, indicating no change in the overall structure of the proteins upon addition of MTSL.

NMR Measurements. Most NMR measurements were performed at 298 K on a Bruker AvanceII 500 MHz spectrometer. In addition, measurements of R_2 relaxation rates were repeated at 800 MHz at the Brandeis University Nuclear Magnetic Resonance Facility. Both spectrometers are equipped with TCI HCN z-gradient cryoprobes. Proton chemical shifts were referenced directly to internal 3-(trimethylsilyl)-1-propanesulfonic acid, sodium salt (DSS), and ^{13}C and ^{15}N chemical shifts were referenced indirectly using the absolute frequency ratios. The NMR spectra were processed with Topspin 1.3 (Bruker) and analyzed with CARA (www.nmr.ch).

^{15}N longitudinal (R_1) and transverse (R_2) relaxation rates and the $^{1}H-^{15}N$ heteronuclear NOE (hetNOE) were measured as described previously (*25*−*27*). The relaxation spectra were processed using NMRPipe version 97.027.12.56 (http://spin.niddk.nih.gov/NMRPipe) (*28*), and peak intensities were analyzed with NMRView version 5.2.2.01 (http://www.onemoonscientific.com/nmrview/download.html) (*29*). The exponential decay function $I = Ae^{-t/R}$ (where I is the peak intensity, A is the amplitude, t is the relaxation delay, and R is R_1 or R_2) was fit to the peak intensities using the jitter function in NMRView to determine the R_1 and R_2 relaxation rates. HetNOEs were calculated by dividing the intensity of the peaks in the spectra without presaturation by the intensity of the peaks in the presaturated spectra.

Chemical Shift Assignment. The following spectra were used to achieve sequence-specific backbone and side chain assignments of all aliphatic residues (*30*): 2D $^{1}H-^{15}N$ HSQC, 3D HNCACB, 3D CBCA(CO)NH, 3D CC(CO)NH, 3D HNCO, 3D HN(CA)CO, 3D HNCA (DARPP-32_{1-118} only), 3D HBHA(CO)NH, 3D ^{15}N-resolved $^{1}H-^{1}H$ NOESY (mixing time of 175 ms), and 3D ^{15}N-resolved $^{1}H-^{1}H$ TOCSY (mixing time of 60 ms). Chemical shift assignments of I-2_{9-164}, DARPP-32_{1-118}, and pDARPP-32_{1-118} were deposited in the BMRB as entries 15179, 15176, and 15865, respectively.

Chemical Shift Indexing and Secondary Structure Propensity. Secondary Structure Propensity (SSP) (*31*) was used to calculate both the chemical shift indices (CSI) and secondary structure propensities (ssp) of I-2_{9-164}, DARPP-32_{1-118}, and pDARPP-32_{1-118} using the $(C\alpha_{exp} - C\beta_{exp}) - (C\alpha_{database} - C\beta_{database})$ method (*32*). The RefDB (*33*), Wang and Jardetzky (*34*), and Wishart (*35*) random coil databases were used in calculations. Data from residues before prolines were excluded; in addition, ssp scores were calculated with a seven-residue moving-average window size.

Analysis of Relaxation Results. ProtScale, on the ExPASy bioinformatics server (http://us.expasy.org), was used to calculate the hydrophobicity profiles using the Abraham and Leo scale (*36*), the bulkiness profiles, and the average area buried on transfer from standard state to folded protein (AABUF) profiles (*37*). In each case, a seven-residue moving-average window size was used and the weight of the window edges was set to 100% compared to the center; values were scaled for ease of visualization. The segmental motion model for the prediction of random coil R_2 relaxation rates was calculated as described previously (*38, 39*), using a chain persistence length of 7 and an R_2^{int} constant of 0.225. Additional relaxation analysis information is provided in the Supporting Information.

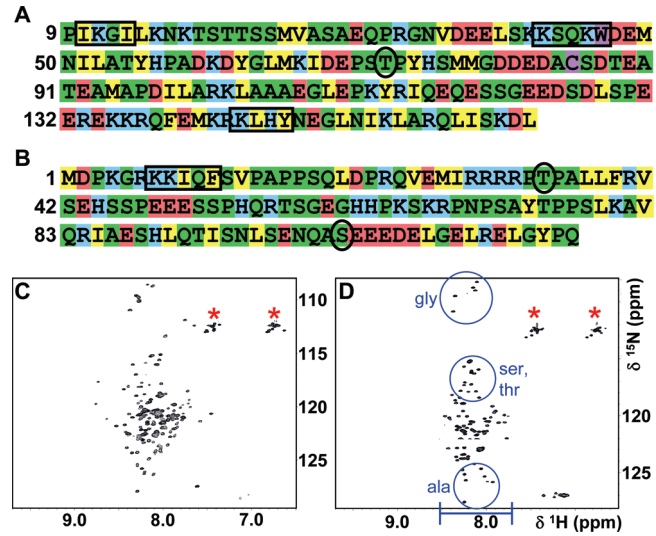

FIGURE 1: Sequence bias and 2D $^{1}H-^{15}N$ HSQC spectra demonstrate that I-2_{9-164} and DARPP-32_{1-118} are intrinsically unstructured. Sequences of (A) I-2_{9-164} and (B) DARPP-32_{1-118} are colored according to Dyson and Wright to highlight the amino acid residue preferences of IUPs (*43*). Green denotes small residues, uncharged hydrophilic residues, and proline residues (Asn, Gln, Ser, Thr, Gly, Ala, and Pro), yellow hydrophobic residues (Val, Leu, Ile, Phe, and Tyr), red acidic residues (Asp and Glu), blue basic residues (Lys, Arg, and His), and purple low-frequency residues (Cys and Trp). Black boxes indicate sequences important for PP1 binding: residues 10−13 (IKGI), 42−46 (KSQKW), and 144−147 (KLHY) in I-2_{9-164} and residues 7−11 (KKIQF) in DARPP-32_{1-118}. Black circles show important phosphorylation sites: Thr^{72} (GSK3) in I-2_{9-164} and Thr^{34} (PKA) and Ser^{102} (CK2) in DARPP-32_{1-118}. 2D $^{1}H-^{15}N$ HSQC spectra are shown for (C) I-2_{9-164} and (D) DARPP-32_{1-118}. The blue bar in panel D indicates the lack of dispersion in the ^{1}H dimension of unstructured proteins, compared to the considerably wider dispersion of peaks in the ^{1}H dimension of structured proteins. Blue circles in panel D demonstrate the amino acid-specific clustering of peaks in unstructured proteins. Red asterisks indicate side chain NH_2 groups of Asn and Gln.

Hydrodynamic Radius Assessed with Dynamic Light Scattering Measurements. DLS measurements using a Viscotek model 802 dynamic light scattering instrument (Viscotek Corp., Houston, TX) were performed to measure the hydrodynamic radius (R_h) of I-2_{9-164} and DARPP-32_{1-118} (25 °C). Numerous empirically derived power factors have been established for folded and denatured proteins (*40, 41*). By direct comparison of the estimated radius for folded and unfolded proteins, protein compaction factors $[C = (R_h^{unfold} - R_h)/(R_h^{unfold} - R_h^{native})]$ were calculated.

RESULTS

I-2_{9-164} and DARPP-32_{1-118} have a sequence bias, with frequent Gln, Ser, Pro, Glu, Lys, and Gly residues (disorder-inducing amino acids) and few hydrophobic residues (Figure 1A,B), suggesting they belong to the family of intrinsically unstructured proteins (IUPs). This is in agreement with the reports of Huang et al. (*22*) and Lin et al. (*21*), which first described the sequence-specific backbone assignments of I-2_{1-172} and DARPP-32_{1-118}, respectively.

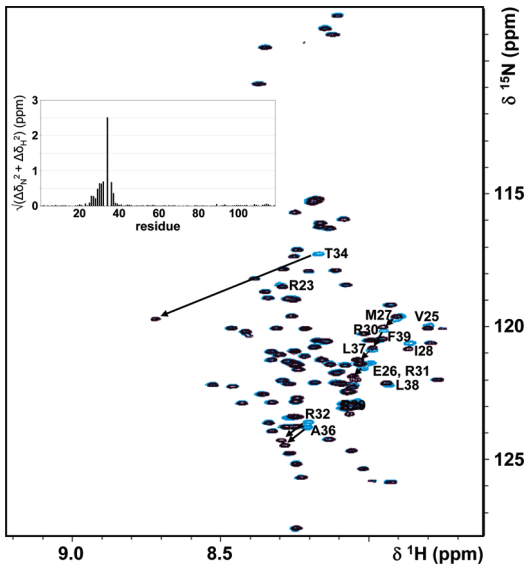

FIGURE 2: Phosphorylation of Thr[34] on DARPP-32$_{1-118}$ does not alter the conformation of DARPP-32$_{1-118}$. Overlay of 2D $^{1}H-^{15}N$ HSQC spectra of DARPP-32$_{1-118}$ (blue) with pDARPP-32$_{1-118}$ (black); changes in the $^{1}H^{N}$ and ^{15}N chemical shifts between the DARPP-32$_{1-118}$ and pDARPP-32$_{1-118}$ 2D $^{1}H-^{15}N$ HSQC spectra are shown in the inset. Peak shifts in the pDARPP-32$_{1-118}$ spectrum are minor, with the exception of that of Thr[34], and are restricted to residues within the vicinity of the phosphorylation site. Residues with peak shifts are indicated with residue numbers and arrows.

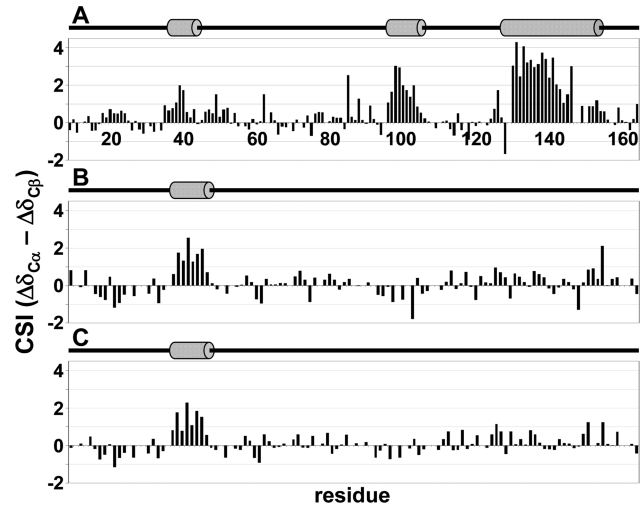

FIGURE 3: CSI scores of (A) I-2$_{9-164}$, (B) DARPP-32$_{1-118}$, and (C) pDARPP-32$_{1-118}$ indicate the presence of transient structural preferences in I-2$_{9-164}$ and DARPP-32$_{1-118}$; preferences are not significantly affected by Thr[34] phosphorylation of DARPP-32$_{1-118}$. The $\delta C\alpha - \delta C\beta$ CSI is reported, calculated using the RefDB (*33*) random coil database. Positive deviations from random coil values indicate transient α-helices. Cartoon representations above each indicate the presence of transient α-helices, as determined by ssp scores (Figure 4), with gray cylinders.

NMR spectroscopy is the only atomic-resolution technique that can be used to investigate the structural and dynamical characteristics of IUPs (*42*). An IUP "structure" has been described as an ensemble of interconverting conformers, often with preferences for certain secondary structure elements and long-range interactions, collectively termed transient structure. A growing body of evidence has shown that this transient structure is correlated with function (*43*). 2D $^{1}H-^{15}N$ HSQC spectra of I-2$_{9-164}$ and DARPP-32$_{1-118}$ are shown in Figure 1C,D; the limited peak dispersion in the ^{1}H dimension indicates that they are in fact unstructured. While it has been shown that I-2$_{1-172}$ and DARPP-32$_{1-118}$ are intrinsically unstructured (*21, 22*), a detailed analysis of their unstructured states, including extensive study of local and, most importantly, long-range transient structure, has not been reported. Furthermore, while previous studies have indicated that the overall conformation of DARPP-32$_{1-118}$ is not affected by Thr[34] phosphorylation (*44*), this has not been studied in molecular detail. Figure 2 shows the overlay of the DARPP-32$_{1-118}$ and pDARPP-32$_{1-118}$ 2D $^{1}H-^{15}N$ HSQC spectra and also a chemical shift difference analysis. This clearly shows that chemical shift changes between the two spectra are limited to the immediate vicinity of Thr[34]. Finally, though I-2$_{9-164}$ and DARPP-32$_{1-118}$ are unstructured, they are active, as shown by their ability to bind PP1 (Supporting Information).

I-2$_{9-164}$ and DARPP-32$_{1-118}$ Have Preferred Secondary Structure. To understand the basis of IUP−PP1 recognition, it is important to elucidate any transient structural preferences of the unbound IUPs, including local structural propensities and long distance interactions, as these might be the critical signatures of their interactions with PP1. NMR chemical shifts are highly sensitive to φ and ψ angle propensities. Therefore, subtracting random coil chemical shifts from experimental chemical shifts ($\Delta\delta$), known as the chemical shift index (CSI) (*32, 35, 45*), is a powerful tool for detecting local regions of transient secondary structure in IUPs. It is known that different nuclei exhibit differential sensitivity toward certain $\varphi-\psi$ combinations; i.e., Cα chemical shifts are far more sensitive to α-helical behavior, and Cβ shifts are more sensitive to β-sheet behavior. Furthermore, $\delta C\alpha$ is positive in a helix and negative in extended structures, while $\delta C\beta$ is the opposite (negative and positive, respectively). Therefore, throughout this work, we used ($C\alpha_{exp} - C\beta_{exp}$) − ($C\alpha_{database} - C\beta_{database}$) values (*32*) to ensure that no single secondary structure propensity is either over- or underemphasized. Positive deviations from random coil values represent preferred α-helical conformations, whereas negative deviations from random coil values represent preferred β-strand or extended structure regions. The $\delta C\alpha - \delta C\beta$ CSI values for I-2$_{9-164}$, DARPP-32$_{1-118}$, and pDARPP-32$_{1-118}$, calculated using the RefDB random coil chemical shift database, are shown in Figure 3. Areas of significantly populated transient α-helices are detected in both I-2$_{9-164}$ and DARPP-32$_{1-118}$; no significant change in transient secondary structure is seen upon Thr[34] phosphorylation of DARPP-32$_{1-118}$ (Figures 2 and 3C).

In fully formed secondary structure, certain amino acid types give stronger CSIs than others. A secondary structure propensity (ssp) score (*31*) normalizes this by calculation of the ratio of the experimental CSI for each residue to the CSI for that specific amino acid type in fully formed secondary structures. This calculation provides an estimate of the percent of time each transient secondary structure element is populated, where an ssp score of 1 indicates an α-helix populated 100% of the time and an ssp score of −1 indicates extended structure populated 100% of the time. We consider areas of transient structure significant if five or more sequential residues have ssp scores of >20%. The ssp scores for I-2$_{9-164}$, DARPP-32$_{1-118}$, and pDARPP-32$_{1-118}$ are shown in the top portions of panels A−C of Figure 4, respectively; transient α-helices are indicated by gray cylinders above the

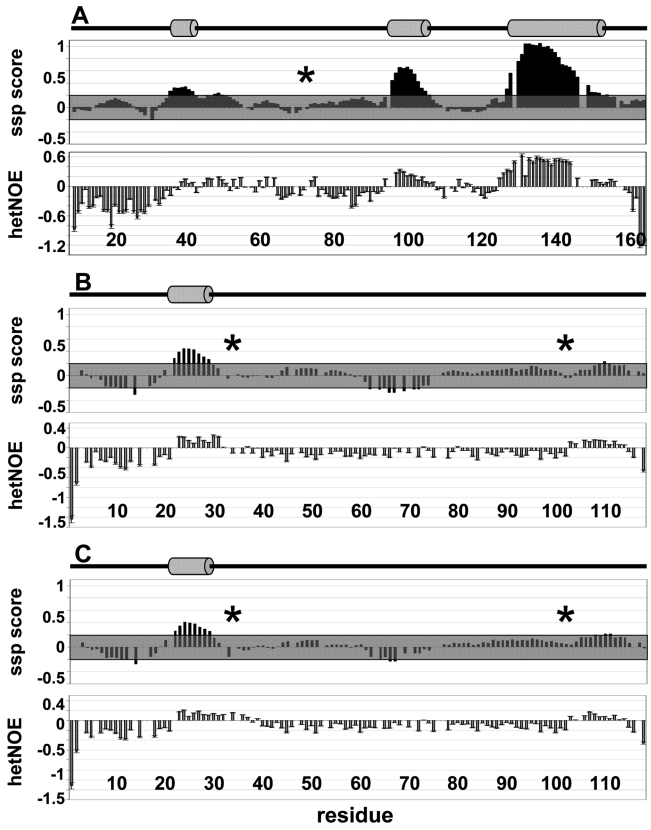

FIGURE 4: ssp scores and $^{15}N-^{1}H$ NOE (hetNOE) data indicate regions of transient structure and reduced backbone motions in I-2_{9-164}, DARPP-32_{1-118}, and pDARPP-32_{1-118}. The size of the region of backbone restriction is increased upon Thr^{34} phosphorylation of DARPP-32_{1-118}. (A) I-2_{9-164} ssp (top) and $^{15}N-^{1}H$ NOE (bottom), (B) DARPP-32_{1-118} ssp (top) and $^{15}N-^{1}H$ NOE (bottom), and (C) pDARPP-32_{1-118} ssp (top) and $^{15}N-^{1}H$ NOE (bottom). Areas of transient structure are considered significant if five or more residues have an ssp score of greater than 0.2, indicating a transient α-helix, or less than −0.2, indicating a region with extended structure. Cartoon representations above the ssp scores indicate the presence of transient α-helices with gray cylinders. Transient α-helices correspond well with regions of restricted backbone motions (positive $^{15}N-^{1}H$ NOEs), and an additional region of restricted motion is found in the C-terminus of DARPP-32_{1-118}. Phosphorylation of DARPP-32 Thr^{34} extends the region of restricted backbone motion and makes the single region of transient extended structure insignificant. Regions of structurally insignificant ssp scores (−0.2 to 0.2) are shown in gray boxes. Asterisks indicate known phosphorylation sites important for PP1 interaction and inhibition: Thr^{72} (GSK3) in I-2_{9-164} and Thr^{34} (PKA) and Ser^{102} (CK2) in DARPP-32_{1-118}.

graphs. Three structural hotspots can be detected in I-2_{9-164}: residues 36−42, 96−106, and 127−154, with residues populating the α-helical conformation space ∼30, 48, and 67% of the time, respectively. Importantly, residues 132−138 have >98% α-helical character based on this analysis. Indeed, this strong helical character is supported by experimentally identified H^N-H^N NOE cross-peaks between residues 132 and 138 in the 3D ^{15}N-resolved $^{1}H-^{1}H$ NOESY spectrum. In DARPP-32_{1-118}, one transient helix is detected: residues 22−29, populated ∼36% of the time, are located immediately N-terminal to the highly conserved Thr^{34} PKA phosphorylation site whose phosphorylation is required for PP1 inhibition. Phosphorylation of Thr^{34} slightly decreases the average percent of time this transient helix is populated from 36 to 33%. Additionally, one region of transient extended structure is detected in DARPP-32_{1-118} between residues 62 and 72, populated on average ∼24% of the time. pDARPP-32_{1-118} does not exhibit ssp scores indicative of significantly populated transient structure in this region.

Flexibility Highlights Potential Important Functional Regions in DARPP-32 and I-2. To further examine these IUPs beyond local structure and to gain insight into the molecular foundation for their preferred transient structures, we carried out autocorrelated ^{15}N relaxation experiments, including measurement of $^{15}N-^{1}H$ NOE and ^{15}N longitudinal (R_1) and transverse (R_2) relaxation rates. The data from these experiments report on the flexibility of the backbone along the protein chain. Larger $^{15}N-^{1}H$ NOEs indicate restricted backbone motions, while small or even negative $^{15}N-^{1}H$ NOEs indicate increased high-frequency backbone mobility. In structured proteins, $^{15}N-^{1}H$ NOE values are positive and follow a flattened bell-shaped curve with the termini exhibiting slightly more flexibility than the remainder of the chain. In contrast, most $^{15}N-^{1}H$ NOE values are negative in unfolded proteins, indicating a high degree of backbone mobility. The bottom portions of panels A−C of Figure 4 show the $^{15}N-^{1}H$ NOEs for I-2_{9-164}, DARPP-32_{1-118}, and pDARPP-32_{1-118}, respectively. Rigid regions (positive $^{15}N-^{1}H$ NOE) of I-2_{9-164} and DARPP-32_{1-118} correlate remarkably with the transient α-helices, confirming the presence of preferred structure in these regions (*15, 46*). In I-2_{9-164}, positive $^{15}N-^{1}H$ NOEs extend beyond the first transient helix (residues 36−42) to include residues up to Tyr^{55}, indicating restricted motion well beyond the transient helix. Phosphorylation of Thr^{34} on DARPP-32_{1-118} increases the rigidity of this region, as seen by the extension of positive $^{15}N-^{1}H$ NOEs beyond the transient helix to residue 37 (positive $^{15}N-^{1}H$ NOEs end at residue 32 in DARPP-32_{1-118}). In addition, residues 103−114 of DARPP-32_{1-118} and pDARPP-32_{1-118} exhibit reduced flexibility that is not mirrored by significant ssp values. Interestingly, Ser^{102} is a known CK2 phosphorylation site, whose phosphorylation has been reported to enhance phosphorylation of Thr^{34}. A group of negatively charged amino acids trails the Ser^{102} phosphorylation site which may contribute to this increased backbone rigidity. Furthermore, although they do not meet our strict criteria for transient structure, residues 109−111 have an average ssp score of 0.21, which may contribute to the localized rigidity.

Testing the Molecular Foundations for Preferred Conformation and Restricted Dynamics. To gain insight into the molecular foundation for these IUPs' preferred transient structures, autocorrelated R_1 and R_2 relaxation data were recorded in addition to the $^{15}N-^{1}H$ NOE data. The interpretation of relaxation rates in IUPs is different from that in structured proteins because internal motions in structured proteins occur on a time scale different from that of the global motion of the protein; thus, and consistent with previous studies, we interpreted the data with spectral density mapping at three frequencies [$J(0)$, $J(0.87\omega_H)$, and $J(\omega_N)$ (Supporting Information)]. The main contributions to $J(0)$ come from both picosecond to nanosecond ($^{15}N-^{1}H$ NOE) and slower nanosecond to millisecond (R_2, among others) backbone motions, and it has been shown that the latter may be responsible for the deviations of R_2 rates from predicted random coil behavior in IUPs (*47*). Consequently, we focus here on the qualitative analysis of R_2 values since they are especially sensitive to local structure variations. The mea-

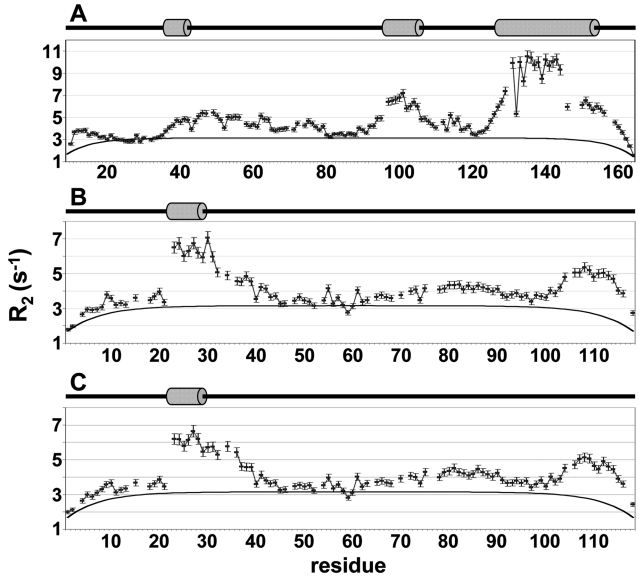

FIGURE 5: Experimental R_2 relaxation rates of I-2_{9-164} and DARPP-32_{1-118} cannot be described using a model for random coil polymers. Experimental R_2 relaxation rates of (A) I-2_{9-164}, (B) DARPP-32_{1-118}, and (C) pDARPP-32_{1-118} are shown as black squares with error bars; rates calculated using the segmental motion model for random coil polymers of the same length are shown as solid black lines. Cartoon representations above each indicate the presence of transient α-helices with gray cylinders, based on ssp scores (Figure 4).

surement of the R_2 relaxation rates at two magnetic fields (500 and 800 MHz) ensured that conformational exchange can likely be excluded as the reason for the deviations of R_2 rates in our IUPs. The R_2 relaxation rates of I-2_{9-164}, DARPP-32_{1-118}, and pDARPP-32_{1-118} are shown in Figure 5. With the exception of the region near the Thr^{34} phosphorylation site, shown by $^{15}N-^{1}H$ NOEs to be more rigid upon phosphorylation, the R_2 relaxation rates of DARPP-32_{1-118} and pDARPP-32_{1-118} agree well. Figure 5 also includes predicted R_2 relaxation rates for random coil proteins of the respective lengths of I-2_{9-164} and DARPP-32_{1-118}, calculated using the segmental motion model. This model was previously shown to accurately predict the R_2 relaxation rates of denatured proteins (*39*); however, it does not predict the R_2 relaxation rates of I-2_{9-164} or DARPP-32_{1-118} within reasonable error.

Therefore, different residue-specific properties such as hydrophobicity, bulkiness, and average area buried upon folding (AABUF) were used to determine whether inherent characteristics of the protein sequence provide the basis for the experimentally detected deviations from random coil behavior in I-2_{9-164} and DARPP-32_{1-118} (Supporting Information). These parameters have been recommended previously to predict these deviations in denatured and unstructured proteins (*48*). In our case, it can be readily seen that for weakly populated transient local structure states, such as $helix_{22-29}$ in DARPP-32_{1-118} or $helix_{36-42}$ in I-2_{9-164}, AABUF profiles correlate well with the experimental R_2 profiles. Therefore, the dynamics of these weakly populated states are dictated by the individual residue-specific characteristics of side chain size and hydrophobicity. However, strongly populated secondary structure elements, such as $helix_{127-154}$ in I-2_{9-164}, can only be correlated in profile, not in magnitude, indicating that cooperativity between residues in a highly populated transient helix, while not directly measureable using CSI data, most likely dominates over individual amino acid properties.

DARPP-32_{1-118} and I-2_{9-164} Exhibit a Preferred Transient Three-Dimensional Structure. IUPs have more extended 3D topologies than folded proteins; however, long-range contacts may still be present, and preferred 3D topologies may play an essential role in the distinct interactions between PP1 and its regulatory proteins. NOE spectroscopy, the most common and reliable source for structure information of folded proteins, cannot be used for IUPs due to their high intrinsic flexibilities. Therefore, dynamic light scattering was used to rapidly asses the hydrodynamic radii of these proteins to determine their overall compactness (*40*). These measurements demonstrate that the inhibitor proteins are ~30% more compact than extended polymer chains of the same length (Supporting Information). Therefore, long-range interactions likely occur in our IUPs and might contribute to their distinct topologies and PP1 binding selectivities.

To gain thorough molecular insight into the preferred 3D topologies of these two IUPs, we used the paramagnetic spin-label MTSL [(1-oxyl-2,2,5,5-tetramethyl-3-pyrroline-3-methyl)methanethiosulfonate] which covalently attaches to free sulfhydryl groups (*49*). Spin-labels cause substantial line broadening of the resonances of spins within ~20 Å of the labeling site through paramagnetic relaxation enhancement (*50*−*52*). Along the protein chain, the ratio of the peak intensity, i.e., in a 2D $^{1}H-^{15}N$ HSQC spectrum, of the paramagnetic sample to that of the diamagnetic sample is correlated with the spatial distance of each residue from the spin-label (*53*). However, an IUP is a highly flexible conformational ensemble; therefore, the ratio is an average ratio for the distance of the spin-label from that residue in the ensemble. A ratio of 1 indicates no relaxation enhancement or that the particular residue is not within 20 Å of the spin-label; a ratio of 0 indicates that the residue is very close to the spin-label in many structures in the ensemble. Because of the innate high backbone flexibility of our IUPs, we did not extract quantitative distances from these measurements; instead, we used them to obtain qualitative descriptions of the preferred 3D topologies of our IUPs.

I-2_{9-164}, DARPP-32_{1-118}, and pDARPP-32_{1-118} were spin labeled at their wild-type cysteine residues (C85 and C72). Additionally, four single-cysteine mutants of I-2_{9-164} and DARPP-32_{1-118} were spin labeled on the basis of the results of the wild-type spin labeling experiments to further test their overall topologies (raw data in the Supporting Information). The paramagnetic spin-label data were translated into contact heat maps and topological models of our IUPs. It is important to point out that these are not computational models of our structures, merely models that were created to improve our understanding of our available short- and long-range data. In I-2_{9-164} (Figure 6A,B), the most prominent observation is a topological core formed around its single tryptophan residue (Trp^{46}), which includes residues ~35−60, ~90−110, and ~150−155. Furthermore, the region just N-terminal to $helix_{127-154}$ spends little time in contact with the rest of I-2_{9-164}. Thus, the first half of $helix_{127-154}$ protrudes from the core of the molecule. DARPP-32_{1-118}'s topology (Figure 6C,D) is distinct from that of I-2_{9-164}. Residues 80−118 spend a significant amount of time as a compact core. The N-terminus, which includes the PP1 binding motif, spends very little time in contact with this core, which may allow it

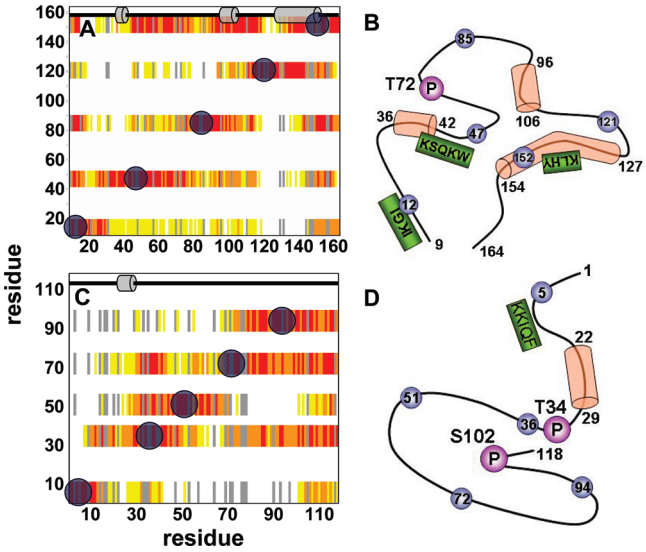

FIGURE 6: Long-range contact (heat) maps indicate the presence of long-range interactions in (A) I-2_{9-164} and (C) DARPP-32_{1-118}. Blue circles designate sites of MTSL spin labeling. Red indicates the largest amount of interaction between the spin-label and the residue (paramagnetic:diamagnetic peak intensity ratio of 0−0.2); orange and yellow indicate a medium amount of interaction (paramagnetic:diamagnetic peak intensity ratios of 0.2−0.4 and 0.4−0.6, respectively), and white indicates very little interaction (paramagnetic:diamagnetic peak intensity ratio of >0.6). Residues without data, including prolines and peaks with severe chemical shift overlap, are colored gray. Cartoon representations across the top of each indicate the presence of secondary structure preferences based on ssp evaluation (Figure 4). (B and D) Topographical representations of unbound I-2_{9-164} and DARPP-32_{1-118}, respectively, with both local and long-range data. Important phosphorylation sites are highlighted (purple circles, described in the legends of Figures 1 and 4), as are PP1 binding motifs (green boxes, described in the legend of Figure 1). Cylinders represent transient α-helices as determined by ssp scores, and blue circles are sites of paramagnetic MTSL spin-labels, which were used to determine the transient tertiary structure of these proteins.

to seek out PP1 as a potential first interaction site. Phosphorylation of Thr^{34} does not affect the profile of long-range contacts on DARPP-32_{1-118} (Supporting Information), as indicated by the similarity in the raw MTSL data between the two forms of DARPP-32_{1-118}.

DISCUSSION

In this study, we have used a variety of approaches to identify the individual structural preferences of two essential protein inhibitors of PP1:I-2_{9-164} and DARPP-32_{1-118}. Additionally, we studied Thr^{34}-phosphorylated DARPP-32_{1-118} to determine whether phosphorylation alters the structural preferences of DARPP-32_{1-118}. Many reported IUPs exhibit transient secondary structure preferences which are important to their function. Indeed, these preferences can often be correlated with fully formed secondary structures following a "folding-upon-binding" transition which can occur when an IUP binds its target molecule (*54*−*56*).

Both tertiary and local structures are present in the unbound states of I-2_{9-164} and DARPP-32_{1-118}. As discussed in further detail below, the results we obtained with I-2_{9-164}, DARPP-32_{1-118}, and pDARPP-32_{1-118} are consistent with previously reported biochemical studies of these proteins in their unbound forms. Taken together, these data allow us to describe potential, distinctive molecular models for the interactions of these two proteins with PP1. The transient structural preferences we report for I-2_{9-164} and DARPP-32_{1-118} are likely to play important roles in their recognition and selectivity for PP1.

Inhibitor-2. Several structure−function studies of I-2 have identified a number of "domains" that are involved in its interaction with PP1 (*15, 17, 19, 57, 58*). A recent study has also presented a crystal structure of the PP1−I-2 complex (*23*). Together, these studies have established that three short regions of I-2 interact directly with PP1: (1) residues 42−54 that contain the $KSQKW^{42-46}$ sequence which interacts with the common (R/K)$x_1x_2x_3$(F/W) motif docking site; (2) residues 11−16, which form a unique N-terminal domain, $KGILKN^{11-16}$, that binds to a site in PP1 adjacent to the $KSQKW^{42-46}$ docking site (*17, 57*); and (3) a C-terminal region between amino acids 128 and 167 that is largely helical in structure and that covers the acidic and hydrophobic grooves as well as the active site of PP1, making a majority of contacts near the active site (*23*).

Our studies of unbound I-2_{9-164} identified three preferred helical regions (residues 36−42, 96−106, and 127−154). In the crystal structure of the PP1−I-2 complex, only ∼25% of all I-2 residues are visible in the experimental electron density map: residues 11−16, 42−54, and 128−167. Residues which compose the first two transient helices in unbound I-2_{9-164} (residues 36−42 and 96−106) have no corresponding experimental electron density map in the crystal structure of the PP1−I-2 complex. Thus, direct comparison between unbound and bound I-2 is not possible for these regions.

The longest of the three preferred helical regions in unbound I-2_{9-164} consists of residues 127−154. Previously, the region containing this helix was biochemically shown to play a critical role in the PP1−I-2 interaction: a peptide of residues 135−151 antagonizes the inhibitory potency of I-2 as well as DARPP-32, indicating that this region of I-2 shares a binding site on PP1 with DARPP-32 (*57*). The crystal structure shows that in the PP1−I-2 complex residues 128−167 bind PP1 in an extended α-helical conformation disrupted only at residues 147−151 (*23*). Residues $LHYNE^{145-149}$ have a dual role, blocking access to PP1's active site and potentially pushing one or both metals out of the active site. Our data show a transient helix in this region of unbound I-2_{9-164}, complementing the crystal structure of I-2 bound to PP1. Taken together, these data indicate that the identified transient helix performs an important role in mediating PP1 binding and inactivation. Importantly, no folding-upon-binding transition is identified for this helix.

While full inhibition of PP1 by I-2 requires the extended helical region at the C-terminus of the protein (residues 128−167), it is clear that the N-terminal region is also involved in the interaction with PP1. Truncation mutagenesis has found that partial fragments of I-2 as short as residues 1−114 (IC_{50} ∼ 10 nM) (*57*) or 1−99 (IC_{50} ∼ 3 nM) (*11*) have strong inhibitory activity comparable to that of full-length I-2 (IC_{50} ∼ 1−2 nM). Thus, N-terminal fragments of I-2 act as potent inhibitors without any occlusion of the active site of PP1. It is possible that although the structure of PP1 is not believed to be grossly affected upon binding targeting or inhibitor proteins (*8, 12, 23*), the N-terminus of I-2 may have an allosteric effect on the active site of PP1. One possibility is that binding of the N-terminal region of I-2 may contribute to the loss of one of the catalytic metals from

PP1, a feature observed in the crystal structure of the PP1−I-2 complex (*23*). Residues LHYNE$^{145-149}$ in the C-terminal helix may then bind to the active site and stabilize the inactive enzyme.

Using paramagnetic spin-labels, it was possible to identify the preferred 3D structure of I-2_{9-164}. It has been proposed that transient local and long-range interactions in IUPs expose primary interaction sites to enable a more effective means of binding to target molecules (*59*). It is our hypothesis that the 3D transient structures of the IUPs studied here provide a molecular signature for their PP1 interactions. A major feature revealed by this analysis of I-2_{9-164} is the preference observed for a topological core formed around its single tryptophan residue (Trp^{46}), which includes residues ~35−60, ~90−110, and ~150−155. The crystal structure of the PP1−I-2 complex shows that Trp^{46} is part of a degenerate common PP1 interaction motif, KSQKW$^{42-46}$. The KSQKW$^{42-46}$ region is located near, but not within, the first transient helix in unbound I-2_{9-164}, allowing this motif to bind the common PP1 interaction site in the required extended conformation.

A second significant 3D feature in I-2_{9-164} is that the N-terminus of the long and significantly populated helix$_{127-154}$ protrudes from I-2_{9-164}'s core. Because of the strong local bias toward secondary structure that is found in unbound and PP1-bound I-2, and the long-range structural features found for unbound I-2_{9-164}, a second potential PP1 interaction scenario could be that helix$_{127-154}$ acts as a primary contact site in I-2_{9-164} which initiates PP1 interaction. This would allow for stabilization of helix$_{127-154}$ and folding of I-2 around the PP1 scaffold. While it is the more popular belief that PP1 regulatory proteins interact first via their common PP1 binding motifs, the existence of a core structure in I-2_{9-164} may allow for a different mode of binding to PP1 where helix$_{127-154}$ instead plays a prominent role as the initial contact site for I-2_{9-164}.

Lastly, phosphorylation of Thr^{72}, a GSK-3β phosphorylation site that is important for the formation of the reactivated ATPMg-dependent PP1 phosphatase complex, has been experimentally shown not to alter the overall structure of unbound I-2_{1-172} (*60*). Our data are consistent with these results since Thr^{72} is part of a longer loop, including residues ~75−90, that shows modest interaction with the I-2_{9-164} core. Residues in this region of I-2_{9-164} are missing from the crystal structure of the PP1−I-2 complex; however, phosphorylation of Thr^{72} on I-2 when bound to PP1 increases the fluorescence anisotropy of I-2, suggesting a conformational change upon phosphorylation of bound I-2 (*61*). Flexibility in this region of I-2 even after binding of PP1 is likely critical to reactivation of the PP1−I-2 complex.

DARPP-32$_{1-118}$. In contrast to I-2_{9-164}, only a single transient helix (residues 22−29) was identified in the pseudosubstrate inhibitor DARPP-32_{1-118}. This region directly connects the two biochemically identified "subdomains" of DARPP-32 that interact with PP1: the common PP1 binding motif (KKIQF$^{7-11}$) (*62*) and the region surrounding Thr^{34}, the essential phosphorylation site whose phosphorylation is needed for strong PP1 inhibition (*15, 62, 63*). While it is possible that secondary structure elements are necessary for some phosphorylation events, structures of PKA in a complex with a pseudosubstrate peptide indicate that the substrate interacts with the active site in an extended manner (*64*−*67*). Furthermore, the Nairn laboratory has previously found that several hydrophobic residues within and near this helix are important for inhibition of PP1. To a lesser extent, the number of residues separating the two subdomains of DARPP-32 are also important: mutations and deletions in this region resulted in an increased IC_{50} for PP1 inhibition by pDARPP-32 (*15*). Therefore, we suggest that the transient helix likely plays an important role in the binding interaction between pDARPP-32 and PP1, acting as a geometric lead to place the pseudosubstrate pThr^{34} at PP1's active site.

PP1 contains three characteristic surface grooves (acidic, hydrophobic, and C-terminal) which emanate from the active site and form the known binding sites for the molecular toxin PP1 inhibitors (*6*). Additionally, these are potential sites of interaction with PP1 substrates. The stretch of residues between helix$_{22-29}$ and Thr^{34} is highly positively charged with numerous arginine residues. This is likely a PP1 interaction signature of DARPP-32, as these residues complement the PP1 acidic groove, which lies between the common interaction site and the active site, in an ideal manner. It has been previously reported that not all areas of this groove are DARPP-32 accessible (*15*); it is thus possible that the transient helix guides DARPP-32 into a certain binding configuration. Thus, in both inhibitors, transient secondary structure likely plays a role in their recognition and binding modes: while helix$_{127-154}$ of I-2 plays a central role in PP1 inhibition by blocking the PP1 active site, helix$_{22-29}$ in DARPP-32 likely guides pThr^{34} into PP1's active site.

A single region of transient extended structure in DARPP-32_{1-118} (residues 62−72) was also identified. One possibility is that transient structure in this region is important for the interaction with PP1 and that it could form a β-sheet with a complementary strand from PP1. However, this is unlikely as pDARPP-32_{1-118} does not exhibit transient extended structure in this region. Another possibility is that because it is N-terminal to the Thr^{75} phosphorylation site (Cdk5) which, when phosphorylated, activates DARPP-32 as an inhibitor of PKA (*68*), the transient structure in this region may play a role in phosphorylation of Thr^{75} or inhibition of PKA.

On the basis of the results from the use of paramagnetic spin-labels, DARRP-32_{1-118} shows a distinctive 3D topology. The C-terminal residues of DARPP-32_{1-118} form a compact core. Residues near the Thr^{34} phosphorylation site show some interaction with the core, and, significantly, also with Ser^{102}. Phosphorylation of Ser^{102} is known to increase the rate of phosphorylation of Thr^{34} (*69*); thus, our data present a topological rationale for this enhancement. Lastly, we show that a region of restricted backbone motion can be detected N-terminal of the Ser^{102} phosphorylation site; this may play a role in the phosphorylation of Ser^{102}. A recent study also indicates that Ser^{102} is involved in regulating the nuclear export of DARPP-32, which contains a potent nuclear exporting sequence that includes the important residues Leu^{108} and Leu^{114}. As Stipanovich et al. (*70*) have shown, when DARPP-32 is phosphorylated at Ser^{102} the nuclear exporting sequence is active and DARPP-32 is pumped out of the nucleus. However, activation of PP2A can dephosphorylate Ser^{102}, prohibiting nuclear export, and thus at steady state gives the appearance of DARPP-32 translocating to the nucleus.

Another important topological feature of DARPP-32_{1-118} is that the common PP1 interaction motif (KKIQF$^{7-11}$) protrudes from the C-terminal core. Mutation of key residues in the motif results in a large decrease in inhibitory potency (*15*). Furthermore, a peptide containing this motif is able to antagonize inhibition of PP1 by pDARPP-32 (*62*), and deletion of the motif significantly decreases the binding affinity of pDARPP-32 for PP1, as seen by surface plasmon resonance (*46*). The freely accessible KKIQF$^{7-11}$ motif may therefore act as an initial docking site for binding to PP1. Docking may stabilize helix$_{22-29}$, which could then wrap around the acidic groove of PP1, and allow placement of the pseudosubstrate pThr^{34} into PP1's active site. Lastly, residues 40−65 form a loosely defined extended loop, as a spin-label on residue 51 is only in the proximity of its neighboring residues. Very little is known about the function of this loop. Ser^{45} is a defined substrate for CK2 in vitro (*69*) and is likely phosphorylated *in vivo* (*71*); additionally, it has been proposed that this site might play a role in increasing the efficacy of phosphorylation by PKA (*69, 71*).

pDARPP-32$_{1-118}$. Phosphorylation of Thr^{34} on DARPP-32 increases its inhibitory potency for PP1 ~1000-fold, similar to the increased inhibitory potency of the myosin phosphatase holoenzyme (MYPT1−PP1 complex) inhibitor CPI-17 upon its phosphorylation at Thr^{38} (*72*−*74*). While DARPP-32 is an unstructured general PP1 inhibitor, CPI-17 is a structured inhibitor specific for the myosin phosphatase holoenzyme, which consists of PP1, the PP1 targeting protein MYPT1, and the M21 accessory subunit. Phosphorylation of CPI-17 induces a conformational change which arranges pThr^{38} on the surface of the inhibitor, poised for interaction with PP1 (*75*). Thus, the phosphorylation-induced conformational change in this structured PP1 inhibitor is critical to its inhibitory role. Fluorescence anisotropy and quenching studies of DARPP-32 have indicated that the overall conformation of DARPP-32 is not altered by phosphorylation of Thr^{34} (*44*). Our data confirm these results by providing molecular-level insight into the structural differences between DARPP-32_{1-118} and pDARPP-32_{1-118}. The length of the single transient helix, helix$_{22-29}$, is not altered by Thr^{34} phosphorylation, though the percent of time this helix is populated decreases slightly from 36 to 33%. No changes in the ^{1}H−^{1}H NOE pattern can be detected upon phosphorylation of Thr^{34} (Supporting Information). Importantly, more residues in this region experience restricted fast time scale backbone motion, indicated by positive ^{15}N−^{1}H NOEs, upon Thr^{34} phosphorylation. This restriction may be due to the strong negative charge of the phosphate group at Thr^{34}. After binding of the common PP1 interaction motif to PP1, this additional backbone restriction may aid in the stabilization of helix$_{22-29}$ and the placement of Thr^{34} in the active site of PP1. In addition, the single, significantly populated region of extended structure in DARPP-32_{1-118}, residues 62−72 indicated by ssp scores of less than −0.2, lost its significance upon phosphorylation of Thr^{34}. This region is highly flexible in both forms of DARPP-32_{1-118}, as indicated by negative ^{15}N−^{1}H NOEs for all residues. Interestingly, fluorescence anisotropy experiments have previously reported that the region near Cys^{72} on DARPP-32 is slightly constrained in motion, though this is not altered by phosphorylation of Thr^{34} (*44*). Our data do not reflect this.

This study shows an important difference between interactions of inhibitor protein with apo-PP1 and those with the myosin phosphatase holoenzyme. DARPP-32_{1-118} does not undergo extensive structural changes upon phosphorylation, in contrast to CPI-17. This indicates that the presence of the strong negative charge of the phosphate group most likely contributes significantly to the binding and inhibition of PP1 by pDARPP-32_{1-118}.

Summary. In summary, we have determined an experimental 3D model for two PP1 inhibitor proteins: DARPP-32 and I-2. The high intrinsic flexibility of these PP1 inhibitor proteins provides a likely rationale for how PP1 can maintain an invariant structure while being selectively inhibited. While interaction between PP1 and its regulatory proteins could be accomplished by two rigid and invariant binding partners, our data highlight the advantages of interactions between a rigid (PP1) and a flexible (inhibitor protein) binding partner. First, the high flexibility of the inhibitor allows for multiple interaction points between the inhibitor and PP1, and also for a large interaction surface with PP1 without the need for excessive protein size. Second, the high intrinsic flexibility might be a way to tune the affinity of this interaction. Most PP1 regulatory proteins bind tightly (low nanomolar K_d). However, due to the large interaction surfaces and the likely occurring loss of degrees of freedom in regulatory proteins upon binding, the entropic cost of this interaction carries an adequate energetic penalty to allow for rapid responses to changing signals of the cell or other regulatory proteins of PP1. Furthermore, while the PP1 binding motif in PP1 regulatory proteins is necessary for binding, their intrinsic structural preferences likely guide their binding interactions with PP1. Lastly, the intrinsic flexibility of these PP1 inhibitors also allows for the simultaneous binding of particular pairs of PP1 targeting and inhibitory proteins to PP1 [which has been proposed for I-2 and spinophilin (*18*)] and therefore provides additional means for rapid modulation of PP1 by cellular signals.

ACKNOWLEDGMENT

We thank Dr. Tun-Li Shen for help with the MS measurements and Dr. Rebecca Page for careful reading of the manuscript.

SUPPORTING INFORMATION AVAILABLE

Further information about methods, including protein expression and purification, NMR analysis, NMR raw data, and DARPP-32_{1-118} and I-2_{9-164} behavior in a crowded environment. This material is available free of charge via the Internet at http://pubs.acs.org.

REFERENCES

1. Moorhead, G. B., Trinkle-Mulcahy, L., and Ulke-Lemee, A. (2007) Emerging roles of nuclear protein phosphatases. *Nat. Rev. Mol. Cell Biol. 8*, 234–244.
2. Cohen, P. T. (2002) Protein phosphatase 1: Targeted in many directions. *J. Cell Sci. 115*, 241–256.
3. Bollen, M. (2001) Combinatorial control of protein phosphatase-1. *Trends Biochem. Sci. 26*, 426–431.
4. Watanabe, T., Huang, H. B., Horiuchi, A., da Cruze Silva, E. F., Hsieh-Wilson, L., Allen, P. B., Shenolikar, S., Greengard, P., and Nairn, A. C. (2001) Protein phosphatase 1 regulation by inhibitors and targeting subunits. *Proc. Natl. Acad. Sci. U.S.A. 98*, 3080–3085.

5. Meiselbach, H., Sticht, H., and Enz, R. (2006) Structural analysis of the protein phosphatase 1 docking motif: Molecular description of binding specificities identifies interacting proteins. *Chem. Biol. 13*, 49–59.
6. Holmes, C. F., Maynes, J. T., Perreault, K. R., Dawson, J. F., and James, M. N. (2002) Molecular enzymology underlying regulation of protein phosphatase-1 by natural toxins. *Curr. Med. Chem. 9*, 1981–1989.
7. Honkanen, R. E., and Golden, T. (2002) Regulators of serine/threonine protein phosphatases at the dawn of a clinical era. *Curr. Med. Chem. 9*, 2055–2075.
8. Goldberg, J., Huang, H. B., Kwon, Y. G., Greengard, P., Nairn, A. C., and Kuriyan, J. (1995) Three-dimensional structure of the catalytic subunit of protein serine/threonine phosphatase-1. *Nature 376*, 745–753.
9. Kita, A., Matsunaga, S., Takai, A., Kataiwa, H., Wakimoto, T., Fusetani, N., Isobe, M., and Miki, K. (2002) Crystal structure of the complex between calyculin A and the catalytic subunit of protein phosphatase 1. *Structure 10*, 715–724.
10. Maynes, J. T., Bateman, K. S., Cherney, M. M., Das, A. K., Luu, H. A., Holmes, C. F., and James, M. N. (2001) Crystal structure of the tumor-promoter okadaic acid bound to protein phosphatase-1. *J. Biol. Chem. 276*, 44078–44082.
11. Egloff, M. P., Johnson, D. F., Moorhead, G., Cohen, P. T., Cohen, P., and Barford, D. (1997) Structural basis for the recognition of regulatory subunits by the catalytic subunit of protein phosphatase 1. *EMBO J. 16*, 1876–1887.
12. Terrak, M., Kerff, F., Langsetmo, K., Tao, T., and Dominguez, R. (2004) Structural basis of protein phosphatase 1 regulation. *Nature 429*, 780–784.
13. Svenningsson, P., Nishi, A., Fisone, G., Girault, J. A., Nairn, A. C., and Greengard, P. (2004) DARPP-32: An integrator of neurotransmission. *Annu. Rev. Pharmacol. Toxicol. 44*, 269–296.
14. Greengard, P., Allen, P. B., and Nairn, A. C. (1999) Beyond the dopamine receptor: The DARPP-32/protein phosphatase-1 cascade. *Neuron 23*, 435–447.
15. Huang, H. B., Horiuchi, A., Watanabe, T., Shih, S. R., Tsay, H. J., Li, H. C., Greengard, P., and Nairn, A. C. (1999) Characterization of the inhibition of protein phosphatase-1 by DARPP-32 and inhibitor-2. *J. Biol. Chem. 274*, 7870–7878.
16. DePaoli-Roach, A. A., and Lee, F. T. (1985) Phosphoprotein phosphatase inhibitor-2 is phosphorylated at both serine and threonine residues in mouse diaphragm. *FEBS Lett. 183*, 423–429.
17. Connor, J. H., Frederick, D., Huang, H., Yang, J., Helps, N. R., Cohen, P. T., Nairn, A. C., DePaoli-Roach, A., Tatchell, K., and Shenolikar, S. (2000) Cellular mechanisms regulating protein phosphatase-1. A key functional interaction between inhibitor-2 and the type 1 protein phosphatase catalytic subunit. *J. Biol. Chem. 275*, 18670–18675.
18. Terry-Lorenzo, R. T., Elliot, E., Weiser, D. C., Prickett, T. D., Brautigan, D. L., and Shenolikar, S. (2002) Neurabins recruit protein phosphatase-1 and inhibitor-2 to the actin cytoskeleton. *J. Biol. Chem. 277*, 46535–46543.
19. Park, I. K., and DePaoli-Roach, A. A. (1994) Domains of phosphatase inhibitor-2 involved in the control of the ATP-Mg-dependent protein phosphatase. *J. Biol. Chem. 269*, 28919–28928.
20. Sakashita, G., Shima, H., Komatsu, M., Urano, T., Kikuchi, A., and Kikuchi, K. (2003) Regulation of type 1 protein phosphatase/inhibitor-2 complex by glycogen synthase kinase-3β in intact cells. *J. Biochem. 133*, 165–171.
21. Lin, T. H., Huang, Y. C., Chin, M. L., Chen, Y. C., Jeng, H. H., Lin, F. M., Shiao, M. S., Horiuchi, A., Greengard, P., Nairn, A. C., and Huang, H. B. (2004) ^{1}H, ^{15}N, and ^{13}C resonance assignments of DARPP-32 (dopamine and cAMP-regulated phosphoprotein, Mr. 32,000): A protein inhibitor of protein phosphatase-1. *J. Biomol. NMR 28*, 413–414.
22. Huang, H. B., Chen, Y. C., Tsai, L. H., Wang, H., Lin, F. M., Horiuchi, A., Greengard, P., Nairn, A. C., Shiao, M. S., and Lin, T. H. (2000) Backbone ^{1}H, ^{15}N, and ^{13}C resonance assignments of inhibitor-2: A protein inhibitor of protein phosphatase-1. *J. Biomol. NMR 17*, 359–360.
23. Hurley, T. D., Yang, J., Zhang, L., Goodwin, K. D., Zou, Q., Cortese, M., Dunker, A. K., and DePaoli-Roach, A. A. (2007) Structural basis for regulation of protein phosphatase 1 by inhibitor-2. *J. Biol. Chem. 282*, 28874–28883.
24. Peti, W., and Page, R. (2007) Strategies to maximize heterologous protein expression in *Escherichia coli* with minimal cost. *Protein Expression Purif. 51*, 1–10.
25. Kay, L. E., Torchia, D. A., and Bax, A. (1989) Backbone dynamics of proteins as studied by ^{15}N inverse detected heteronuclear NMR spectroscopy: Application to staphylococcal nuclease. *Biochemistry 28*, 8972–8979.
26. Akke, M., and Palmer, A. G. (1996) Monitoring macromolecular motions on microsecond to millisecond time scales by $R_{1\rho}-R_1$ constant relaxation time NMR spectroscopy. *J. Am. Chem. Soc. 118*, 911–912.
27. Palmer, A. G., and Case, D. A. (1992) Molecular dynamics analysis of NMR relaxation in a zinc-finger peptide. *J. Am. Chem. Soc. 114*, 9059–9067.
28. Delaglio, F., Grzesiek, S., Vuister, G. W., Zhu, G., Pfeifer, J., and Bax, A. (1995) NMRPipe: A multidimensional spectral processing system based on UNIX pipes. *J. Biomol. NMR 6*, 277–293.
29. Johnson, B. A. (2004) Using NMRView to visualize and analyze the NMR spectra of macromolecules. *Methods Mol. Biol. 278*, 313–352.
30. Sattler, J., Schleucher, J., and Griesinger, C. (1999) Heteronuclear multidimensional NMR experiments for the structure determination of proteins in solution employing pulsed field gradients. *Prog. NMR Spectrosc. 34*, 93–158.
31. Marsh, J. A., Singh, V. K., Jia, Z., and Forman-Kay, J. D. (2006) Sensitivity of secondary structure propensities to sequence differences between α- and γ-synuclein: Implications for fibrillation. *Protein Sci. 15*, 2795–2804.
32. Spera, S., and Bax, A. (1991) Empirical correlation between protein backbone conformation and Ca and Cb ^{13}C nuclear magnetic resonance chemical shifts. *J. Am. Chem. Soc. 113*, 5490–5492.
33. Zhang, H., Neal, S., and Wishart, D. S. (2003) RefDB: A database of uniformly referenced protein chemical shifts. *J. Biomol. NMR 25*, 173–195.
34. Wang, Y., and Jardetzky, O. (2002) Probability-based protein secondary structure identification using combined NMR chemical-shift data. *Protein Sci. 11*, 852–861.
35. Wishart, D. S., Bigam, C. G., Holm, A., Hodges, R. S., and Sykes, B. D. (1995) ^{1}H, ^{13}C and ^{15}N random coil NMR chemical shifts of the common amino acids. I. Investigations of nearest-neighbor effects. *J. Biomol. NMR 5*, 67–81.
36. Abraham, D. J., and Leo, A. J. (1987) Extension of the fragment method to calculate amino acid zwitterion and side chain partition coefficients. *Proteins: Struct., Funct., Genet. 2*, 130–152.
37. Rose, G. D., Geselowitz, A. R., Lesser, G. J., Lee, R. H., and Zehfus, M. H. (1985) Hydrophobicity of amino acid residues in globular proteins. *Science 229*, 834–838.
38. Schwalbe, H., Fiebig, K. M., Buck, M., Jones, J. A., Grimshaw, S. B., Spencer, A., Glaser, S. J., Smith, L. J., and Dobson, C. M. (1997) Structural and dynamical properties of a denatured protein. Heteronuclear 3D NMR experiments and theoretical simulations of lysozyme in 8 M urea. *Biochemistry 36*, 8977–8991.
39. Wirmer, J., Peti, W., and Schwalbe, H. (2006) Motional properties of unfolded ubiquitin: A model for a random coil protein. *J. Biomol. NMR 35*, 175–186.
40. Wilkins, D. K., Grimshaw, S. B., Receveur, V., Dobson, C. M., Jones, J. A., and Smith, L. J. (1999) Hydrodynamic radii of native and denatured proteins measured by pulse field gradient NMR techniques. *Biochemistry 38*, 16424–16431.
41. Kohn, J. E., Millett, I. S., Jacob, J., Zagrovic, B., Dillon, T. M., Cingel, N., Dothager, R. S., Seifert, S., Thiyagarajan, P., Sosnick, T. R., Hasan, M. Z., Pande, V. S., Ruczinski, I., Doniach, S., and Plaxco, K. W. (2004) Random-coil behavior and the dimensions of chemically unfolded proteins. *Proc. Natl. Acad. Sci. U.S.A. 101*, 12491–12496.
42. Eliezer, D. (2007) Characterizing residual structure in disordered protein states using nuclear magnetic resonance. *Methods Mol. Biol. 350*, 49–67.
43. Dyson, H. J., and Wright, P. E. (2005) Intrinsically unstructured proteins and their functions. *Nat. Rev. Mol. Cell Biol. 6*, 197–208.
44. Neyroz, P., Desdouits, F., Benfenati, F., Knutson, J. R., Greengard, P., and Girault, J. A. (1993) Study of the conformation of DARPP-32, a dopamine- and cAMP-regulated phosphoprotein, by fluorescence spectroscopy. *J. Biol. Chem. 268*, 24022–24031.
45. Wishart, D. S., Sykes, B. D., and Richards, F. M. (1992) The chemical shift index: A fast and simple method for the assignment of protein secondary structure through NMR spectroscopy. *Biochemistry 31*, 1647–1651.
46. Lin, T. H., Tsai, P. C., Liu, H. T., Chen, Y. C., Wang, L. H., Hsieh, F. K., and Huang, H. B. (2005) Characterization of the Protein Phosphatase 1-Binding Motifs of Inhibitor-2 and DARPP-32 by Surface Plasmon Resonance. *J. Biochem. 138*, 697–700.

47. Klein-Seetharaman, J., Oikawa, M., Grimshaw, S. B., Wirmer, J., Duchardt, E., Ueda, T., Imoto, T., Smith, L. J., Dobson, C. M., and Schwalbe, H. (2002) Long-range interactions within a nonnative protein. *Science 295*, 1719–1722.
48. Schwarzinger, S., Wright, P. E., and Dyson, H. J. (2002) Molecular hinges in protein folding: The urea-denatured state of apomyoglobin. *Biochemistry 41*, 12681–12686.
49. Lietzow, M. A., Jamin, M., Jane Dyson, H. J., and Wright, P. E. (2002) Mapping long-range contacts in a highly unfolded protein. *J. Mol. Biol. 322*, 655–662.
50. Schmidt, P. G., and Kuntz, I. D. (1984) Distance measurements in spin-labeled lysozyme. *Biochemistry 23*, 4261–4266.
51. Gillespie, J. R., and Shortle, D. (1997) Characterization of long-range structure in the denatured state of staphylococcal nuclease. II. Distance restraints from paramagnetic relaxation and calculation of an ensemble of structures. *J. Mol. Biol. 268*, 170–184.
52. Gillespie, J. R., and Shortle, D. (1997) Characterization of long-range structure in the denatured state of staphylococcal nuclease. I. Paramagnetic relaxation enhancement by nitroxide spin labels. *J. Mol. Biol. 268*, 158–169.
53. Teilum, K., Kragelund, B. B., and Poulsen, F. M. (2002) Transient structure formation in unfolded acyl-coenzyme A-binding protein observed by site-directed spin labelling. *J. Mol. Biol. 324*, 349–357.
54. Dyson, H. J., and Wright, P. E. (2002) Coupling of folding and binding for unstructured proteins. *Curr. Opin. Struct. Biol. 12*, 54–60.
55. Tompa, P. (2005) The interplay between structure and function in intrinsically unstructured proteins. *FEBS Lett. 579*, 3346–3354.
56. Radhakrishnan, I., Perez-Alvarado, G. C., Dyson, H. J., and Wright, P. E. (1998) Conformational preferences in the Ser133-phosphorylated and non-phosphorylated forms of the kinase inducible transactivation domain of CREB. *FEBS Lett. 430*, 317–322.
57. Yang, J., Hurley, T. D., and DePaoli-Roach, A. A. (2000) Interaction of inhibitor-2 with the catalytic subunit of type 1 protein phosphatase. Identification of a sequence analogous to the consensus type 1 protein phosphatase-binding motif. *J. Biol. Chem. 275*, 22635–22644.
58. Park, I. K., Roach, P., Bondor, J., Fox, S. P., and DePaoli-Roach, A. A. (1994) Molecular mechanism of the synergistic phosphorylation of phosphatase inhibitor-2. Cloning, expression, and site-directed mutagenesis of inhibitor-2. *J. Biol. Chem. 269*, 944–954.
59. Csizmok, V., Bokor, M., Banki, P., Klement, E., Medzihradszky, K. F., Friedrich, P., Tompa, K., and Tompa, P. (2005) Primary contact sites in intrinsically unstructured proteins: The case of calpastatin and microtubule-associated protein 2. *Biochemistry 44*, 3955–3964.
60. Lin, T. H., Chen, Y. C., Chyan, C. L., Tsay, L. H., Tang, T. C., Jeng, H. H., Lin, F. M., and Huang, H. B. (2003) Phosphorylation by glycogen synthase kinase of inhibitor-2 does not change its structure in free state. *FEBS Lett. 554*, 253–256.
61. Picking, W. D., Kudlicki, W., Kramer, G., Hardesty, B., Vandenheede, J. R., Merlevede, W., Park, I. K., and DePaoli-Roach, A. (1991) Fluorescence studies on the interaction of inhibitor 2 and okadaic acid with the catalytic subunit of type 1 phosphoprotein phosphatases. *Biochemistry 30*, 10280–10287.
62. Kwon, Y. G., Huang, H. B., Desdouits, F., Girault, J. A., Greengard, P., and Nairn, A. C. (1997) Characterization of the interaction between DARPP-32 and protein phosphatase 1 (PP-1): DARPP-32 peptides antagonize the interaction of PP-1 with binding proteins. *Proc. Natl. Acad. Sci. U.S.A. 94*, 3536–3541.
63. Hemmings, H. C., Jr., Nairn, A. C., Elliott, J. I., and Greengard, P. (1990) Synthetic peptide analogs of DARPP-32 (Mr 32,000 dopamine- and cAMP-regulated phosphoprotein), an inhibitor of protein phosphatase-1. Phosphorylation, dephosphorylation, and inhibitory activity. *J. Biol. Chem. 265*, 20369–20376.
64. Kim, C., Vigil, D., Anand, G., and Taylor, S. S. (2006) Structure and dynamics of PKA signaling proteins. *Eur. J. Cell Biol. 85*, 651–654.
65. Meinkoth, J. L., Alberts, A. S., Went, W., Fantozzi, D., Taylor, S. S., Hagiwara, M., Montminy, M., and Feramisco, J. R. (1993) Signal transduction through the cAMP-dependent protein kinase. *Mol. Cell. Biochem. 127−128*, 179–186.
66. Taylor, S. S., Kim, C., Vigil, D., Haste, N. M., Yang, J., Wu, J., and Anand, G. S. (2005) Dynamics of signaling by PKA. *Biochim. Biophys. Acta 1754*, 25–37.
67. Taylor, S. S., Yang, J., Wu, J., Haste, N. M., Radzio-Andzelm, E., and Anand, G. (2004) PKA: A portrait of protein kinase dynamics. *Biochim. Biophys. Acta 1697*, 259–269.
68. Nairn, A. C., Svenningsson, P., Nishi, A., Fisone, G., Girault, J. A., and Greengard, P. (2004) The role of DARPP-32 in the actions of drugs of abuse. *Neuropharmacology 47* (1), 14–23.
69. Girault, J. A., Hemmings, H. C., Jr., Williams, K. R., Nairn, A. C., and Greengard, P. (1989) Phosphorylation of DARPP-32, a dopamine- and cAMP-regulated phosphoprotein, by casein kinase II. *J. Biol. Chem. 264*, 21748–21759.
70. Stipanovich, A., Valjent, E., Matamales, M., Nishi, A., Ahn, J. H., Maroteaux, M., Bertran-Gonzalez, J., Brami-Cherrier, K., Enslen, H., Corbille, A. G., Filhol, O., Nairn, A. C., Greengard, P., Herve, D., and Girault, J. A. (2008) A phosphatase cascade by which rewarding stimuli control nucleosomal response. *Nature 453*, 879–884.
71. Jin, M., Bateup, H., Padovan, J. C., Greengard, P., Nairn, A. C., and Chait, B. T. (2005) Quantitative analysis of protein phosphorylation in mouse brain by hypothesis-driven multistage mass spectrometry. *Anal. Chem. 77*, 7845–7851.
72. Desdouits, F., Cheetham, J. J., Huang, H. B., Kwon, Y. G., da Cruz e Silva, E. F., Denefle, P., Ehrlich, M. E., Nairn, A. C., Greengard, P., and Girault, J. A. (1995) Mechanism of inhibition of protein phosphatase 1 by DARPP-32: Studies with recombinant DARPP-32 and synthetic peptides. *Biochem. Biophys. Res. Commun. 206*, 652–658.
73. Ohki, S., Eto, M., Kariya, E., Hayano, T., Hayashi, Y., Yazawa, M., Brautigan, D., and Kainosho, M. (2001) Solution NMR structure of the myosin phosphatase inhibitor protein CPI-17 shows phosphorylation-induced conformational changes responsible for activation. *J. Mol. Biol. 314*, 839–849.
74. Ohki, S., Eto, M., Shimizu, M., Takada, R., Brautigan, D. L., and Kainosho, M. (2003) Distinctive solution conformation of phosphatase inhibitor CPI-17 substituted with aspartate at the phosphorylation-site threonine residue. *J. Mol. Biol. 326*, 1539–1547.
75. Eto, M., Kitazawa, T., Matsuzawa, F., Aikawa, S., Kirkbride, J. A., Isozumi, N., Nishimura, Y., Brautigan, D. L., and Ohki, S. Y. (2007) Phosphorylation-induced conformational switching of CPI-17 produces a potent myosin phosphatase inhibitor. *Structure 15*, 1591–1602.

BI801308Y